

Photoinduced insulator-to-metal phase transition in VO₂ crystalline films and model of dielectric susceptibility

S. Lysenko, V. Vikhnin,* F. Fernandez, A. Rua, and H. Liu†

Department of Physics, University of Puerto Rico, Mayaguez, Puerto Rico 00681, USA

(Received 18 August 2006; revised manuscript received 3 December 2006; published 15 February 2007)

A light-induced insulator-to-metal ultrafast phase transition (PT) was observed in VO₂ thin films deposited on single-crystal sapphire and amorphous glass substrates. The PT and optical properties of VO₂ were characterized by transient reflection, absorption, and transient grating nonlinear optical measurements. VO₂ films deposited on crystalline substrates are spatially ordered and show noticeable anisotropy in optical response upon PT. Structural and optical properties are dependent on the shear plane of the sapphire substrate. Significant twinning was found for VO₂ deposited on a (001)Al₂O₃ substrate while a VO₂ film on (012)Al₂O₃ is highly textured, without detectable twinning. VO₂ dielectric susceptibility is described by a proposed model. The V-O-V charge transfer was considered as a major process contributing to the linear and nonlinear dielectric susceptibility. The PT time and relaxation dynamics were found to be dependent on the film morphology and concentration of structural defects.

DOI: [10.1103/PhysRevB.75.075109](https://doi.org/10.1103/PhysRevB.75.075109)

PACS number(s): 78.47.+p, 71.30.+h, 78.20.-e

I. INTRODUCTION

The metal-insulator phase transition in vanadium dioxide (VO₂) is one of the key problems of solid-state physics which has been extensively studied in recent years. The first-order insulator-to-metal (*I-M*) phase transition (PT) of VO₂ can be initiated by simple heating or by light illumination.^{1,2} During the *I-M* PT the VO₂ lattice transforms from monoclinic phase with crystallographic space group C_{2h}^5 to tetragonal (rutile) phase of group D_{4h}^{14} . As a result, the physical characteristics of VO₂, such as conductivity, magnetic susceptibility, Seebeck coefficients, and optical constants, undergo a considerable change.³⁻⁷ The thermally induced PT occurs at a temperature about $T_c=340$ K, demonstrating hysteresis of various physical properties versus temperature. The width and shape of the hysteresis strongly depend on the internal structure of VO₂. The light-induced PT is nonthermal and extremely fast: the *I-M* optical switching occurs within ~ 100 fs.⁸ Therefore the light-induced PT in VO₂ thin films is very important for practical applications such as light-controlled solid-state optical switchers and diffractive elements, storage devices, infrared laser cavity mirrors with switchable reflectivity, smart optical windows, ultrafast light-controlled electronic devices, etc.⁹⁻¹⁵

From the scientific perspective the mechanism of the phase transition phenomenon in vanadium dioxide is still not clear. The driving force for the PT and the contribution of the electron-lattice interactions as well as electron-electron correlations to the PT have been under discussion in numerous investigations. It is expected that the role played by electron-electron correlations in VO₂ is considerable in order to stabilize the insulator phase, especially for Cr-doped VO₂.⁶ On the other hand, the experimentally observed spontaneous vanadium tilting and paring along the *c* axis during a PT clearly demonstrates the Peierls mechanism of $d_{||}$ -band splitting. The PT in VO₂ is first order, and the lattice symmetry cannot be broken directly by the Hubbard mechanism. However, the lattice distortion could be considered a consequence of the correlation gap opening by the Hubbard mechanism. Such a

type of PT where electron correlations are dominant in the PT mechanism was considered in Refs. 16 and 17. It is also expected that the lattice relaxation could be strongly influenced by structural inhomogeneities.^{18,19}

In the insulator phase VO₂ is paramagnetic, while other correlated vanadium oxides such as V₂O₃ and V₆O₁₃ show antiferromagnetic ordering. The electron-lattice interaction which includes the charge-density waves shows the lattice instability of metallic VO₂ at the *R* point of the Brillouin zone.²⁰ The tendency to condensation of the soft phonon mode at the *R* point near the PT temperature (Peierls mechanism) was observed in VO₂ by diffuse x-ray scattering experiments.²¹ A strong direct electron-phonon interaction and structurally driven *I-M* PT were found experimentally on the subpicosecond time scale in femtosecond pump-probe experiments.⁸ The VO₂ band structure and importance of the lattice distortion in the PT mechanism was considered in terms of crystal-field theory by Goodenough²² and quantitatively described in Refs. 20, 23, and 24 in terms of band theory. Two different mechanisms of thermally induced and light induced PT in VO₂ have been proposed in Refs. 25-27. The spontaneous charge transfer (CT) O²⁻ \rightarrow V⁵⁺ interacting with the lattice can be considered as the order parameter for a thermally induced PT. It was shown that the carrier-induced screening of the CT in metallic VO₂ plays an important role in the PT. The driving force for a light-induced PT could be related to the vibronic exciton-controlled mechanism. According to this model the consecutive excitation of Frenkel and in-cluster vibronic Wannier-Mott excitons results in a resonance *I-M* PT process.

In this paper we investigate the phase transition dynamics and polarization-dependent optical properties of VO₂ crystalline films upon femtosecond laser excitation. A model for VO₂ dielectric susceptibility based on consideration of light-assisted charge transfer is proposed. Optical studies of light-induced PT were conducted by the transient grating technique and pump-probe transmission and reflection measurements. In order to compare the VO₂ physical properties, VO₂ films with equal thicknesses were grown by the

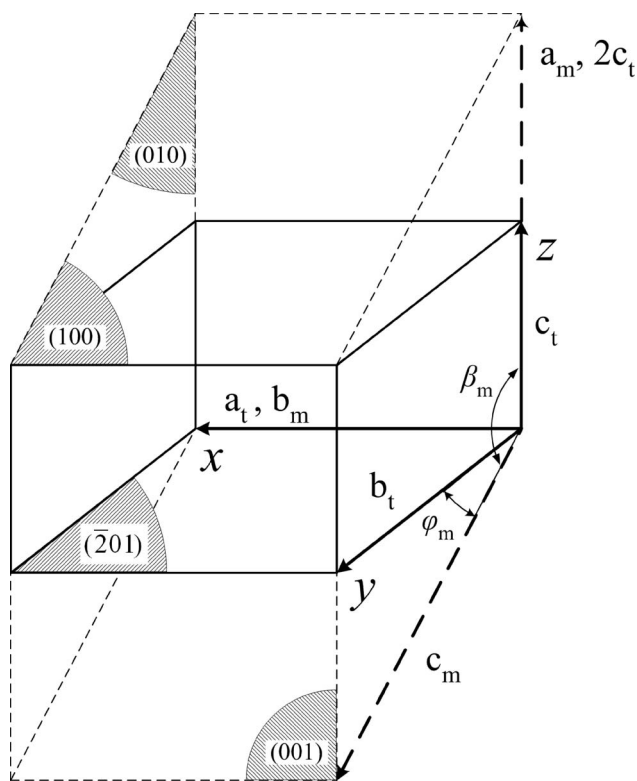


FIG. 1. The unit cell of VO₂ crystal. Dashed lines represent monoclinic cell. The tetragonal cell is shown by solid lines.

pulsed laser deposition (PLD) technique. Significant structural and optical anisotropy will be demonstrated for the films deposited on crystalline sapphire substrates. It will be shown that the excited-state dynamics and PT time are sensitive to the film structure.

II. LATTICE STRUCTURE AND DIELECTRIC SUSCEPTIBILITY

A. Optical indicatrix and dielectric tensor

The VO₂ unit cell for the tetragonal and monoclinic phases is shown in Fig. 1. In the tetragonal phase the structural lattice parameters are $a_t = b_t = 4.55 \text{ \AA}$ and $c_t = 2.88 \text{ \AA}$,^{28,29} and all axial angles are 90°. During the metal-insulator PT the unit cell is doubled and slightly distorted. As a result the lattice parameters in the monoclinic phase become $a_m = 5.743 \text{ \AA}$, $b_m = 4.517 \text{ \AA}$, and $c_m = 5.375 \text{ \AA}$.³⁰ The axial angle between a_m and c_m is $\beta_m = 122.61^\circ$. Crystallographic planes for monoclinic VO₂ are marked in Fig. 1. Taking into account the small twist of the unit cell during PT, the a_t and c_t directions are assumed to coincide with b_m and a_m , respectively; the a_m , c_m , b_t , and c_t axes are located in the same plane (010).

Optical properties of crystalline vanadium dioxide are strongly related to the lattice symmetry. Since the VO₂ unit cell is not cubic, light propagation through the VO₂ crystal is anisotropic and can be described in terms of the optical indicatrix (i.e., ellipsoidal surface where the radius vector corresponds to the index of refraction). The imaginary part of

the VO₂ refractive index is several times less than the real part.³ Therefore, it is expected that the real part produces the main contribution to the VO₂ optical anisotropy. Nevertheless, absorption is not small in the optical spectral range. The dielectric tensor $\hat{\epsilon}$ of VO₂ is complex and can be simply described in the coordinate system xyz superposed on tetragonal crystallographic axes, as shown in Fig. 1. The tensor $\hat{\epsilon}$ for an absorbing crystal with tetragonal crystallographic symmetry takes a simple diagonal form with components $\epsilon_{xx}^t = \epsilon_{yy}^t = \epsilon_{\perp}^t$ and $\epsilon_{zz}^t = \epsilon_{\parallel}^t$.³¹ After the PT to the monoclinic phase, the dielectric tensor changes significantly. Nondiagonal components $\epsilon_{xy}^m = \epsilon_{yx}^m$ and $\epsilon_{xz}^m = \epsilon_{zx}^m$ appear due to twisting of the unit cell. However, these components are significantly smaller than the others and can be ignored. By neglecting an optical gyrotropy, the dielectric tensors $\hat{\epsilon}^t$ and $\hat{\epsilon}^m$ for the tetragonal and monoclinic phase, respectively, can be defined as

$$\hat{\epsilon}^t \cong \begin{pmatrix} \epsilon_{\perp}^t & 0 & 0 \\ 0 & \epsilon_{\perp}^t & 0 \\ 0 & 0 & \epsilon_{\parallel}^t \end{pmatrix}, \quad \hat{\epsilon}^m \cong \begin{pmatrix} \epsilon_{xx}^m & 0 & 0 \\ 0 & \epsilon_{yy}^m & \epsilon_{yz}^m \\ 0 & \epsilon_{zy}^m & \epsilon_{zz}^m \end{pmatrix}. \quad (1)$$

In the metallic tetragonal phase the optical indicatrix is an ellipsoid with optical principal axis oriented along the z direction; the other two axes—along x and y —are equal. The cross section of this ellipsoid by the $(\bar{2}01)$ plane is a circle. In the insulator monoclinic phase, however, the ellipsoid has three different axes: one axis coincides with the x direction; the other two orthogonal principal axes are arbitrarily oriented in the (010) plane.

B. Model of dielectric susceptibility taking into account the linear and nonlinear optical response

In transient optical experiments the signal intensity is a function of the light-induced modulation of dielectric constants. The main idea related to the transient optical properties of VO₂ is a charge-transfer contribution to the dielectric susceptibility. Between two adjacent vanadium nuclei there are electron clouds of the oxygen atoms,³² through which the CT in vanadium pair occurs. V-O pairs form electric dipoles, and the V-O distance is critical for the CT. As shown for the tetragonal lattice structure in Fig. 2, the CT occurs along two V-O-V orthogonal directions a_t and b_t in the $(\bar{2}01)$ plane, where only coplanar vanadium and oxygen atoms are represented. Similarly, V-O-V CT occurs along the c_t axis, which is normal to the plane of the figure. In the monoclinic phase the atomic positions are slightly changed, but the V-O-V CT scheme is similar. The CT direction corresponds to the maximal change of the electronic polarizability induced by CT due to the pump laser or probe laser interaction. As a result, the angular dependence of the diffracted signal intensity will be defined by the angle φ between the direction of the field vector \mathbf{E} and each V-O-V CT direction. Obviously, spatial anisotropy of CT will cause anisotropy of dielectric susceptibility.

Let us consider the CT induced by an optical field polarized along a chain of vanadium atoms (directions a_t or b_t in Fig. 2). In terms of harmonic CT model, the VO₂ single-cell

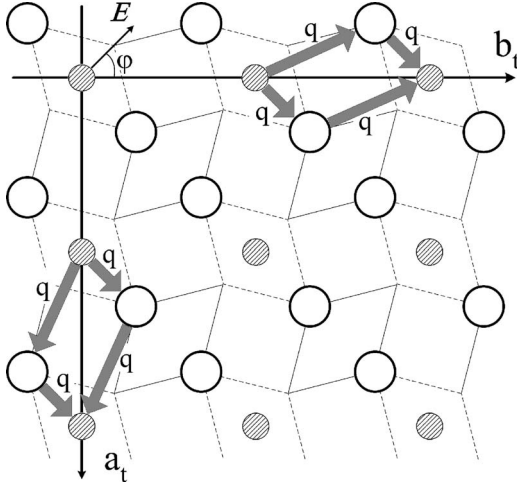


FIG. 2. Diagram shows the cross section of tetragonal VO₂ lattice by the $(\bar{2}01)$ plane. Hatched and open circles represent vanadium and oxygen atoms, respectively. Solid and dashed lines show projection of oxygen octahedrons shifted on half of the lattice constant along the c_t axis. The V-O-V charge transfer is shown by heavy arrows.

charge-transfer potential with respect to the dimensionless CT order parameter q is

$$\delta U_{cell} = \frac{\alpha}{2} q^2 + \Delta q + \frac{\beta}{4} q^4 - qeaE. \quad (2)$$

Here a is a CT length which controls the light-induced dipole moment of CT (i.e., it is the distance between two V ions in Fig. 2), $\alpha = m\omega_{CT}^2 a^2$, ω_{CT} is the CT frequency, and m is the mass coefficient. The parameter Δ is a total excitation energy including Hubbard-type energy. The third term in Eq. (2) is related to the fourth-order anharmonicity for the CT. It should be stressed that this term is an origin of nonlinear optical response of vanadium dioxide. The dielectric susceptibility of a unit cell for a fixed CT direction can be expressed in terms of equilibrium charge transfer:

$$\chi_{cell}(0) = \frac{\partial \mu(E)}{\Omega \partial E} = \frac{ae}{\Omega} \frac{\partial q_{eq}(E)}{\partial E}, \quad (3)$$

where $\mu(E)$ is the dipole moment of the lattice cell and Ω is the cell volume. The equilibrium value of the CT order parameter $q_{eq}(E)$ is determined by minimization of the potential (2) and solution of the following cubic equation:

$$(\Delta - eaE) + \alpha q_{eq} + \beta q_{eq}^3 = 0. \quad (4)$$

The result obtained from Eqs. (3) and (4) shows that the equilibrium values of CT order parameter and dielectric susceptibility are dependent on external electric field. Hence, the dielectric susceptibility represents both linear and nonlinear contributions of CT with respect to electric field strength. The spectral-dependent dielectric susceptibility has Lorentz frequency behavior:

$$\chi_{cell}(\omega) = \chi_{cell}(0) \frac{\omega_{CT}^2}{\omega_{CT}^2 - \omega^2 + i\Gamma\omega}, \quad (5)$$

where Γ is the charge-transfer damping due to charge-transfer—lattice interaction and ω is the light frequency. The mean-field approximation gives a dispersion-type relation for dielectric susceptibility of the CT source for bulk VO₂:

$$\chi(\mathbf{k}, \omega) = \frac{\chi_{cell}(\omega)}{1 - D(\mathbf{k})\chi_{cell}(\omega)}, \quad (6)$$

where $D(\mathbf{k})$ is a dispersion function controlled by Fourier transform of the parameter D_{lm} used in the CT-CT interaction energy between neighboring cells:

$$U_{CT-CT} = -D_{lm} q_l q_m. \quad (7)$$

The mode-softening condition for the charge-transfer-assisted phase transition is

$$D(\mathbf{k}_{BZ})\chi_{cell}(\omega) = 1. \quad (8)$$

The wave vector \mathbf{k}_{BZ} corresponds to the critical point on the boundary of the Brillouin zone and related to the VO₂ cell doubling. Such a PT phenomenon can be treated as a trigger-type effect in VO₂. From a microscopic point of view, the mode-softening and related PT is addressed to the CT-controlled mechanism and can be analyzed in terms of a charge-transfer vibronic exciton phase model.^{33–35} Taking into account the coexistence of dielectric and metallic microregions within the temperature range of the VO₂ phase transition, we can obtain an additional [with respect to the CT effect (5)] free-carrier isotropic contribution to the high-frequency susceptibility:³

$$\chi_{FC}(\omega) = -\frac{\omega_n^2}{\omega^2 + i\omega\omega_c}, \quad (9)$$

where ω_n and ω_c are plasma and free-electron collision frequencies. It could be realized even at room temperature under the condition of an extended hysteresis loop.

III. EXPERIMENTAL DETAILS

A. Thin-film growth

The VO₂ thin films were deposited on amorphous SiO₂ and crystalline Al₂O₃ substrates by the pulsed laser deposition technique. The sapphire substrates were single-crystal slices: (012)Al₂O₃ [R cut, Al₂O₃(R)] and (001)Al₂O₃ [C cut, Al₂O₃(C)]. These different substrates were used in order to create VO₂ thin films with different morphologies. VO₂ films were fabricated in an oxygen and argon atmosphere under a total pressure of ~ 30 mTorr in the vacuum chamber. A metallic vanadium target was evaporated by a pulsed KrF excimer laser (Lambda Physik Compex 110, wavelength $\lambda = 248$ nm, 20-ns pulse duration, 4 J/cm² fluence). The stoichiometry and structural properties of the resulting vanadium oxide films are extremely sensitive to PLD conditions, particularly the O₂/Ar flow speed rate and substrate temperature. Pure phase VO₂ films were formed in the tetragonal phase at O₂ and Ar flow rates of 20 and 5 cm³/min, respec-

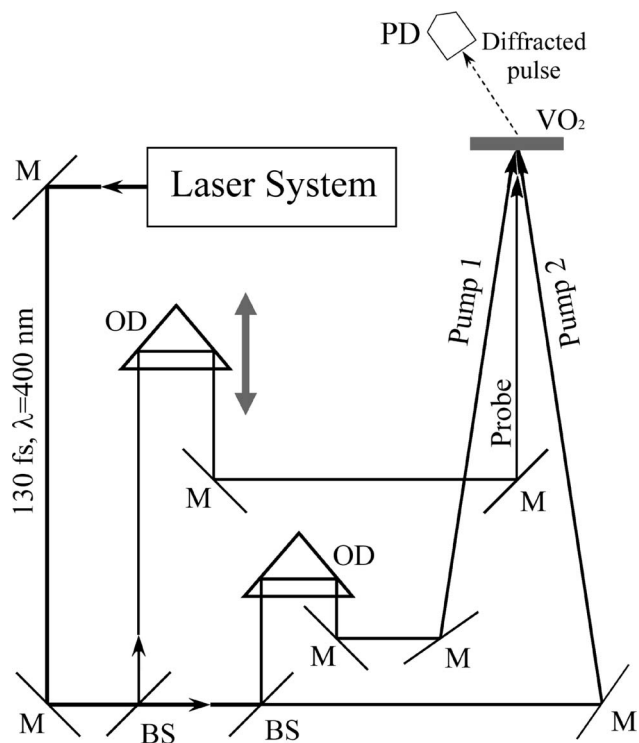


FIG. 3. Experimental setup. *M*, mirror; *OD*, optical delay; *BS*, beam splitter; *PD*, photodetector.

tively. During deposition the substrates were held at a temperature of 840 K. For this work, 30-nm-thick VO_2/SiO_2 , $\text{VO}_2/\text{Al}_2\text{O}_3(\text{R})$, and $\text{VO}_2/\text{Al}_2\text{O}_3(\text{C})$ films were deposited simultaneously in the same PLD run. As a result, these films were created with identical conditions and with equal thicknesses.

B. Methods

The structure of the VO_2 films was determined by angle-resolved x-ray diffraction (XRD) and atomic force microscopy (AFM). The x-ray diffraction measurements were performed in a Bruker D8 Discover diffractometer (Bruker AXS, Karlsruhe, Germany). The area of the sample illuminated by x rays was $\sim 1 \times 5$ mm. The surface geometry was probed by an atomic force microscope (Park Scientific Instruments, Autoprobe CP) using a Si_3N_4 cantilever.

Transmission measurements covering the wavelength range 380–1000 nm were performed with a Hitachi U-2001 spectrophotometer.

The time-resolved transient grating diffraction measurements were conducted in forward geometry. The experimental setup is illustrated in Fig. 3. A Ti:sapphire laser system running at a 50-Hz repetition rate was used as a light source; 120-fs output laser pulses with central wavelength $\lambda = 400$ nm were split by a glass beam splitter into pump and probe pulses. The interference pattern on the sample surface was produced by two equally divided *s*-polarized pump pulses with crossing angle $\theta = 9^\circ$ or $\theta = 22.5^\circ$. As a consequence, a light-induced spatial transient grating was created. The probe pulse impinged the surface at normal incidence

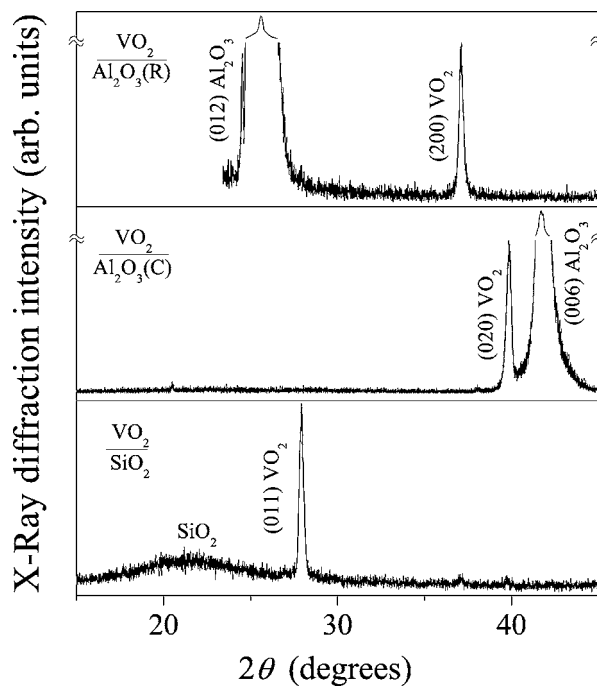


FIG. 4. X-ray diffraction patterns of VO_2 films deposited on crystalline Al_2O_3 and amorphous SiO_2 substrates.

$\theta_{inc} = 0^\circ$ and was focused into a 50- μm spot within the central area of the interference pattern formed by the two crossed pump beams. The diffraction intensity of the probe pulse was monitored as a function of time delay between pump and probe. The timing was controlled by an electromechanical optical delay line mounted on a motorized translation stage. The VO_2 samples were installed on a precision rotation holder.

In pump-probe transmission and reflection measurements only one pump pulse was used. Measurements were conducted at normal incidence of probe pulses. In spectral transient reflectivity measurements white light pulses were used as a probe. The white light continuum was generated by focusing of femtosecond radiation with $\lambda = 800$ nm on a sapphire plate. A monochromator equipped with a photomultiplier tube was employed to measure the spectrum of reflected pulses.

IV. RESULTS AND DISCUSSION

A. Structure of VO_2 films

X-ray diffraction was used in order to analyze the structural properties of vanadium dioxide thin films. The XRD pattern (Fig. 4) shows a pure M_1 phase characterized by a (200) reflection peak at $2\theta = 37.1^\circ$ for $\text{VO}_2/\text{Al}_2\text{O}_3(\text{R})$, (020) reflection at $2\theta = 39.8^\circ$ for $\text{VO}_2/\text{Al}_2\text{O}_3(\text{C})$, and (011) reflection at $2\theta = 27.9^\circ$ for VO_2/SiO_2 samples. No peaks from secondary phases were detected. A broad peak with maximum near $2\theta = 21.5^\circ$ and peaks at $2\theta = 25.6^\circ$ and 41.7° for VO_2/SiO_2 , $\text{VO}_2/\text{Al}_2\text{O}_3(\text{R})$, and $\text{VO}_2/\text{Al}_2\text{O}_3(\text{C})$, respectively, correspond to the substrate contribution to the signal. A sharp peak very close to the substrate (012) peak in Fig. 4

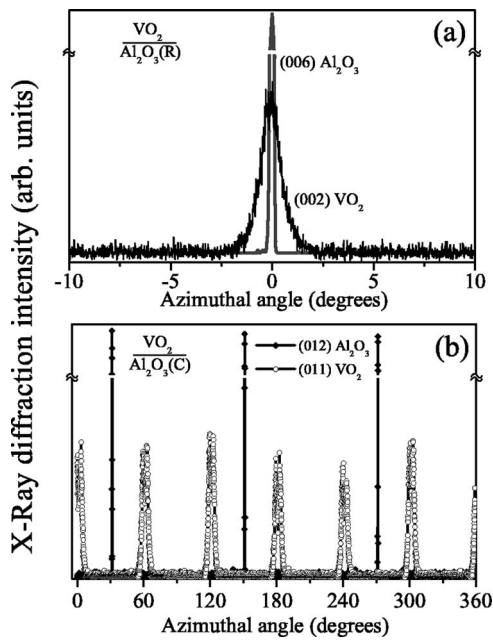


FIG. 5. X-ray diffraction intensity vs azimuthal orientation of the sample for (a) $(006)\text{Al}_2\text{O}_3(R)$ and $(002)\text{VO}_2$ plane of $\text{VO}_2/\text{Al}_2\text{O}_3(R)$ and (b) $(012)\text{Al}_2\text{O}_3(C)$ and $(011)\text{VO}_2$ plane of $\text{VO}_2/\text{Al}_2\text{O}_3(C)$.

corresponds to a ghost reflection of the intense sapphire (012) peak and is due to tungsten impurities in the copper target of the x-ray tube. Thus the x-ray diffraction spectra demonstrate the presence of VO_2 crystallites with different preferred orientations which are strongly dependent on the substrate type: $(100)\text{VO}_2\parallel(012)\text{Al}_2\text{O}_3(R)$, $(010)\text{VO}_2\parallel(001)\text{Al}_2\text{O}_3(C)$, and $(011)\text{VO}_2\parallel\text{SiO}_2$.

In order to study the orientations of the VO_2 films in the surface plane, azimuthal XRD scans (f scans) were conducted for the films on sapphire substrates. The substrate-dependent two-dimensional orientation of the VO_2 lattice was found. The $\text{VO}_2/\text{Al}_2\text{O}_3(R)$ thin film had high structural ordering without detectable crystalline twinning. In the corresponding f scans obtained at the appropriate tilt angles [Fig. 5(a)], only a single $(002)\text{VO}_2$ reflection was found for the film, at the same position as the $(006)\text{Al}_2\text{O}_3(R)$ reflection for the substrate. These data indicate that the orientation of b_m and c_m VO_2 axes in the surface plane is $[010]\text{VO}_2\parallel[100]\text{Al}_2\text{O}_3(R)$ and $[001]\text{VO}_2\parallel[02\bar{1}]\text{Al}_2\text{O}_3(R)$, respectively.

The $\text{VO}_2/\text{Al}_2\text{O}_3(C)$ film, in contrast, demonstrates pronounced twinning. Figure 5(b) shows six $(011)\text{VO}_2$ XRD peaks with 60° symmetry which correspond to a threefold twinned structure with 120° domain walls. Hence, the VO_2 lattice is oriented along three equivalent Al_2O_3 crystallographic directions as $[100]\text{VO}_2\parallel[100]\text{Al}_2\text{O}_3(C)$, $[100]\text{VO}_2\parallel[010]\text{Al}_2\text{O}_3(C)$, and $[100]\text{VO}_2\parallel[\bar{1}\bar{1}0]\text{Al}_2\text{O}_3(C)$. These XRD results are in agreement with data in Refs. 36 and 37.

The surface topography is strongly dependent on mechanisms involved in the PLD process. The AFM studies of the surface provide detailed information on the geometric relief.

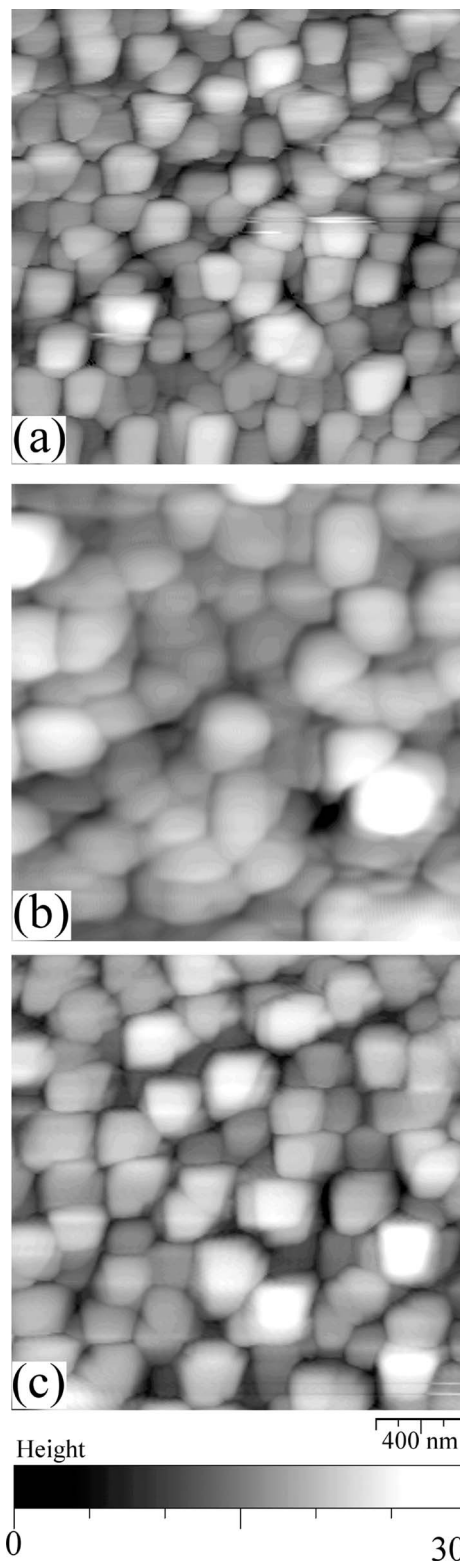


FIG. 6. Atomic force microscope images of VO_2 topography ($2 \times 2 \mu\text{m}^2$ scan): (a) VO_2/SiO_2 , (b) $\text{VO}_2/\text{Al}_2\text{O}_3(R)$, and (c) $\text{VO}_2/\text{Al}_2\text{O}_3(C)$.

The topography of the VO_2 films deposited on different substrates is shown in Figs. 6(a)–6(c). The root-mean-square (rms) roughness evaluated from AFM data for VO_2/SiO_2 , $\text{VO}_2/\text{Al}_2\text{O}_3(R)$, and $\text{VO}_2/\text{Al}_2\text{O}_3(C)$ is 5.4 nm, 5.1 nm, and

5.3 nm, respectively. These quite close rms values appear due to the similar geometry of the films. The average size of VO_2 grains is about 300 nm for all samples. Only slight differences in the topography are distinguishable. The complex surface topography conceals the specific features of different films. Nevertheless, statistical analysis of the surface allows finding significant geometrical regularities and the correlation between surface structures of the films.

Thin-film growth on a substrate depends on numerous PLD factors. In general, film growth in different surface areas is not completely independent, even for growth on amorphous substrates, because this process includes a series of correlated mechanisms such as the mass and heat transfer from one surface point to another and relaxation of mechanical stresses. Therefore the spatial distribution of surface heights $z(u, v)$ for two orthogonal u and v directions is not entirely random. A functional relation between heights at different surface points separated by an interval L is stochastic and can be characterized by the autocorrelation function (ACF).³⁸ The ACF represents a signature of the surface irregularities. Namely, this function represents the change of heights distribution law versus surface shift L . Thus, the ACF provides statistical information about the spatial distribution of surface heights and can be expressed by

$$\text{ACF}(L) = \lim_{\xi \rightarrow \infty} \frac{1}{\delta^2 \xi} \int_{\xi} z(u + L_u, v + L_v) z(u, v) du dv, \quad (10)$$

where ξ is the surface area, δ is the rms roughness, u and v are Cartesian coordinates of the surface, and L_u and L_v are surface shifts from the coordinate origin along u and v directions, respectively.

The autocorrelation analysis of AFM data for our samples shows the isotropic random height distribution for the VO_2 film deposited on an amorphous SiO_2 substrate and significant anisotropy for VO_2 on single-crystal Al_2O_3 . ACF data obtained for $\text{VO}_2/\text{Al}_2\text{O}_3(\text{R})$ and $\text{VO}_2/\text{Al}_2\text{O}_3(\text{C})$ are shown in Fig. 7. For $\text{VO}_2/\text{Al}_2\text{O}_3(\text{R})$ [Fig. 7(a)] the ACF shows oscillations with four pronounced peaks at $L=600$ and 900 nm along two orthogonal directions which are parallel to $[010]\text{VO}_2 \parallel [100]\text{Al}_2\text{O}_3(\text{R})$ and $[001]\text{VO}_2 \parallel [02\bar{1}]\text{Al}_2\text{O}_3(\text{R})$ directions, as determined by XRD. Figure 7(b) is more complex and represents a highly symmetrical ACF with characteristic peaks along preferential directions with $\alpha=30^\circ$ and $\beta=45^\circ$ symmetry.

The oscillation period of the autocorrelation function corresponds to the size of the structural unit which is periodic on the surface. ACF data obtained for $\text{VO}_2/\text{Al}_2\text{O}_3(\text{R})$ indicate strong ordering of surface heights with characteristic sizes of 300 and 600 nm along $[100]\text{Al}_2\text{O}_3(\text{R})$ and $[02\bar{1}]\text{Al}_2\text{O}_3(\text{R})$ substrate crystallographic directions, respectively. Taking into account the XRD results previously discussed, the $\text{VO}_2/\text{Al}_2\text{O}_3(\text{R})$ film can be represented as a non-twinned highly-textured crystalline film with correlated surface irregularities along two crystallographic axes.

The oscillation period of the ACF along marked directions for $\text{VO}_2/\text{Al}_2\text{O}_3(\text{C})$ [Fig. 7(b)] is about 300 nm. It is very likely that the preferential directions which do not coincide with Al_2O_3 crystallographic axes correspond to the twinned

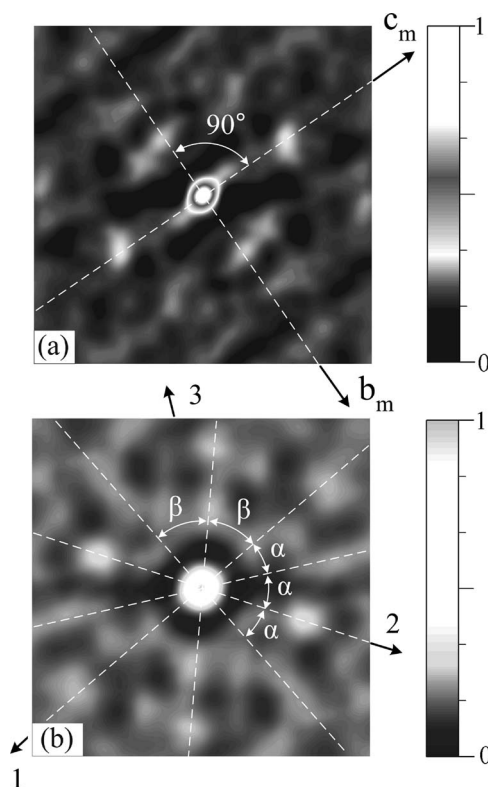


FIG. 7. Autocorrelation function of (a) $\text{VO}_2/\text{Al}_2\text{O}_3(\text{R})$ ($3 \times 3 \mu\text{m}^2$ area) and (b) $\text{VO}_2/\text{Al}_2\text{O}_3(\text{C})$ ($2 \times 2 \mu\text{m}^2$ area). Arrows 1, 2, and 3 correspond to the substrate crystallographic directions $[100]\text{Al}_2\text{O}_3(\text{C})$, $[010]\text{Al}_2\text{O}_3(\text{C})$, and $[\bar{1}\bar{1}0]\text{Al}_2\text{O}_3(\text{C})$, respectively.

structure of the film. ACF data indicate that the local structure of $\text{VO}_2/\text{Al}_2\text{O}_3(\text{C})$ can be represented as a set of twinned VO_2 grains pointing along only two crystallographic directions of the sapphire substrate. Other AFM measurements of the $\text{VO}_2/\text{Al}_2\text{O}_3(\text{C})$ film showed that within different areas of the sample the VO_2 grains also align along the third equivalent crystallographic direction of the $\text{Al}_2\text{O}_3(\text{C})$ substrate. This result is consistent with the XRD results related to threefold twinning of the film. Nevertheless, in most cases the AFM analysis of $2 \times 2 \mu\text{m}^2$ surface areas showed the local orientation of twinned VO_2 grains along only two directions.

In addition to XRD and AFM data, the VO_2 temperature hysteresis was examined by reflection measurements. For VO_2 films on single-crystal Al_2O_3 substrates the hysteresis width was $\Delta T \sim 4$ K, while for VO_2 on amorphous SiO_2 the hysteresis is much broader, with $\Delta T \sim 20$ K. According to Ref. 39, the narrow hysteresis for $\text{VO}_2/\text{Al}_2\text{O}_3(\text{C})$ or $\text{VO}_2/\text{Al}_2\text{O}_3(\text{R})$ corresponds to crystalline films with less structural defects. The broader hysteresis of VO_2/SiO_2 is attributed to numerous oxygen vacancies and significant dispersion in oxygen nonstoichiometry. This result is in agreement with structural data obtained by XRD and AFM.

In conclusion, the $\text{VO}_2/\text{Al}_2\text{O}_3(\text{C})$ film consists of twinned VO_2 crystalline grains while there is no twinning in the $\text{VO}_2/\text{Al}_2\text{O}_3(\text{R})$ film. Hence, the twinning effect and oxygen vacancies cause a number of structural inhomogeneities in $\text{VO}_2/\text{Al}_2\text{O}_3(\text{C})$. Nevertheless, the narrow hysteresis width

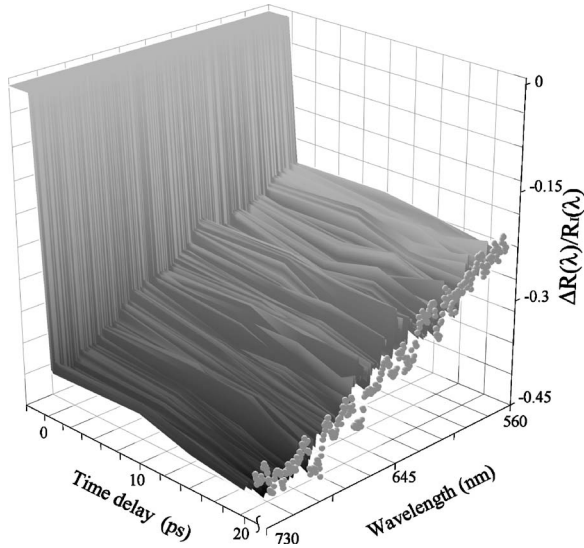


FIG. 8. Normalized change of reflection in optical spectral range after light-induced (temporal dependence) and thermally induced (● symbols, static values) I - M PT in VO_2 film.

($\Delta T \sim 4$ K) obtained for both $\text{VO}_2/\text{Al}_2\text{O}_3(\text{R})$ and $\text{VO}_2/\text{Al}_2\text{O}_3(\text{C})$ is typical for single VO_2 crystal and indicates a relatively high structural quality of these films. However, a very different structural property was observed for VO_2/SiO_2 . Its broader hysteresis along with random distribution of grains on the amorphous substrate indicates a higher concentration of oxygen vacancies, grain interfaces, and elastic tensions in the vicinity of structural defects. Therefore from $\text{VO}_2/\text{Al}_2\text{O}_3(\text{R})$ and $\text{VO}_2/\text{Al}_2\text{O}_3(\text{C})$ to VO_2/SiO_2 films a gradual increase of the structural inhomogeneities can be expected.

B. Spectral properties of VO_2 thin films during a phase transition

The change of the VO_2 optical constants can be induced by ultrafast laser excitation which pumps free carriers to the hybridized π^* and upper $3d_{||}$ bands. This change is associated with the I - M PT. However, additional nonlinearity may occur due to the nonequilibrium distribution of electrons in the conduction band. In order to clarify the relative nonlinear electronic contribution to transient optical properties at the picosecond time scale the light-induced change in reflectivity was measured in comparison to a thermally induced one in a broad spectral range.

The time evolution of the light-induced change in the spectral reflectivity $\Delta R(\lambda)/R_I(\lambda)$ for VO_2/SiO_2 and the reflectivity change induced by heating to 410 K are shown in Fig. 8. Here $\Delta R(\lambda)$ is the change of the reflection coefficient due to a PT and $R_I(\lambda)$ denotes the reflection coefficient of VO_2 in its insulator phase. White-light femtosecond pulses were applied as the probe. The pump laser fluence was $w_p = 30 \text{ mJ/cm}^2$. The reflectivity change after film heating is associated with a complete first-order phase transition. A similar behavior was also found in transient reflection measurements using the pump-probe technique. There was no

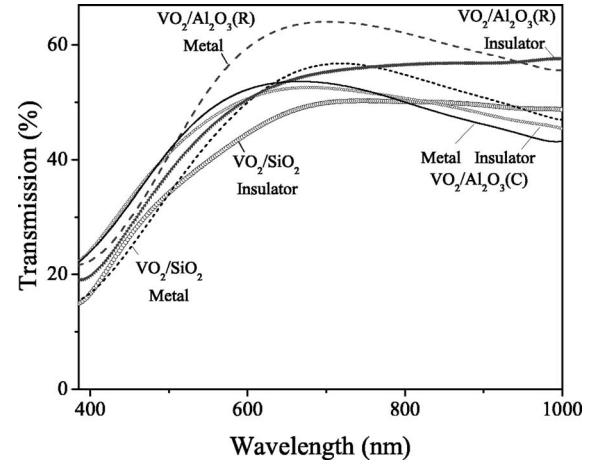


FIG. 9. Transmission spectra for 30-nm-thick VO_2 films for the low- T insulator phase at $T = 295$ K and for the high- T metallic phase at $T = 410$ K.

further relaxation process observed after the light-induced instantaneous change in reflection for any of the spectral components. Comparing the $\Delta R(\lambda)$ process by optical pumping to the process by thermal heating, it is believed that ultrafast laser excitation causes a complete I - M phase transition. The contribution due to optical nonlinearity in total reflection during 0.5–20 ps is negligible. As a consequence, on this time scale the VO_2 dielectric constants can be described in terms of a linear approximation.

As shown above, VO_2 films prepared in the same deposition process are similar in rms roughness and thicknesses, but different in crystallographic orientation and texture with respect to the substrate type. To reveal the effect of spectral optical anisotropy in vanadium dioxide thin films for nonpolarized light, transmission measurements were conducted. The spectral dependences obtained (Fig. 9) are typical for pure VO_2 film and show a strong thermochromic effect for all samples. Also it shows a significant influence of the VO_2 lattice orientation on transmission at temperatures below and above the PT point.

The thin-film model⁴⁰ was applied to estimate the film dielectric constants based on transmission data. It indicates that the imaginary part of the VO_2 refractive index increases after an I - M PT while the optical absorption decreases due to light interference in VO_2 thin film. The relative change in transmission upon a PT is significantly different for different samples (Fig. 9). Such a difference indicates anisotropy of VO_2 optical constants due to different orientation of VO_2 lattice on SiO_2 , $\text{Al}_2\text{O}_3(\text{R})$, and $\text{Al}_2\text{O}_3(\text{C})$ substrates. The effective dielectric constant for nonpolarized light is an averaged value (i) of the components ϵ_{yy}^i , $\epsilon_{yz}^i = \epsilon_{zy}^i$ and ϵ_{zz}^i for $\text{VO}_2/\text{Al}_2\text{O}_3(\text{C})$, (ii) $\epsilon_{(100)}^i$ in the plane (100) for $\text{VO}_2/\text{Al}_2\text{O}_3(\text{R})$, and (iii) $\epsilon_{(011)}^i$ in the plane (011) for VO_2/SiO_2 ; here, the index $i = t, m$ denotes the tetragonal or monoclinic phase, respectively. It should be noted that the dielectric constant $\epsilon_{(011)}^i$ for VO_2/SiO_2 is isotropic due to the isotropic nature of the film deposited on amorphous glass. The maximal and minimal relative changes in transmission are observed for $\text{VO}_2/\text{Al}_2\text{O}_3(\text{R})$ and $\text{VO}_2/\text{Al}_2\text{O}_3(\text{C})$, respec-

tively. This result indicates a larger change in dielectric constants for $\text{VO}_2/\text{Al}_2\text{O}_3(\text{R})$ than that for twinned crystalline $\text{VO}_2/\text{Al}_2\text{O}_3(\text{C})$ film.

C. Phase transition dynamics

Ultrafast transient grating measurements were conducted for 30-nm-thick VO_2 films. An instantaneous light-induced I - M PT occurs within the bright areas of the fringe pattern produced by the two crossed pump beams. Owing to equal thicknesses of the different films, the light-induced PT was realized under the same conditions for all films. The diffraction efficiency of the probe pulse is proportional to the averaged value of the squared deviation in dielectric constant^{41,42} and can be expressed as

$$\eta(t) = \frac{P_{\text{diff}}}{P_{\text{inc}}} \approx \text{OF}(\theta_{\text{inc}}, \theta, \varepsilon, \lambda, d_{\text{film}}) \langle |\Delta\varepsilon(t)|^2 \rangle \quad (11)$$

where P_{diff} and P_{inc} are intensities of diffracted and incident light, respectively, OF is a time-independent optical factor, d_{film} is the film thickness, and $\Delta\varepsilon(t)$ is the light-induced change of dielectric constant. The $\langle \dots \rangle$ brackets denote the spatial averaging. In our experiments OF has a slight dependence on the sample optical anisotropy and is assumed to be constant for all orientations of the sample.

To compare PT and excited-state dynamics for different VO_2 films with equal thickness, time-resolved transient diffraction $\eta(t)$ was measured with constant laser fluence $w_p = 10 \text{ mJ/cm}^2$. The linearly polarized probe pulse impinged the surface at normal incidence. In order to find the polarization dependence of the diffraction signal on the direction of the optical electric field as well as the sample orientation, the samples were placed and fixed at the normal axis.

The light-induced I - M PT dynamics in the transient grating experiment shows two components: it is a light-induced ultrafast phase transition (UPT) occurring on a femtosecond time scale (Fig. 10) followed by a slower PT component which is a continuation of the PT until subnanoseconds (Fig. 11). Strong optical anisotropy could be observed in $\text{VO}_2/\text{Al}_2\text{O}_3(\text{R})$. For the $\text{VO}_2/\text{Al}_2\text{O}_3(\text{C})$ sample, however, a little angular dependence was identified and a fully isotropic signal was observed for VO_2/SiO_2 . Figures 10 and 11 show the transient grating diffraction signal $\eta(t)$ as a function of probe delay. The normalized signal shows a rapid buildup at zero delay, forming a sharp peak followed by subsequent relaxation.

The change of diffraction signal during the PT for all samples (Fig. 10) is correlated to the spectroscopic data (Fig. 9). A noticeable difference appears in the signal intensity for $\text{VO}_2/\text{Al}_2\text{O}_3(\text{C})$ compared to other films. This is related to the different film optical constants, resulting from the different structural orientation of the VO_2 films on different substrates, as shown by XRD. The sharp peaks at zero delay are associated with the nonlinear contribution in dielectric susceptibility $\chi(\mathbf{k}, \omega)$ as was discussed in Sec. II A significant contribution to $\eta(t)$ during the I - M UPT is caused by a change in intra-atomic equilibrium positions upon laser excitation.^{18,19} When the UPT is completed, the diffraction

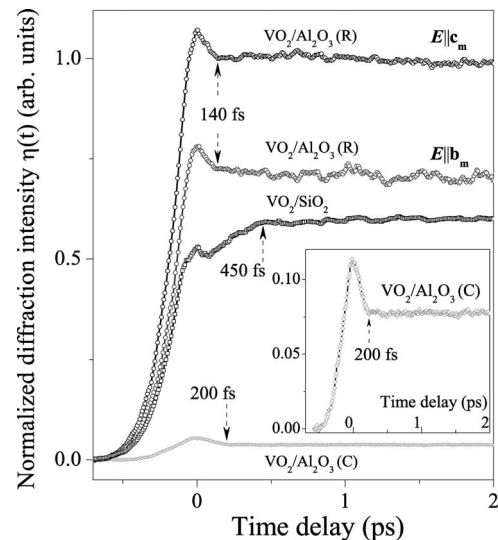


FIG. 10. Transient grating signal versus probe-pulse delay upon a light-induced insulator-to-metal phase transition. The inset shows a zoomed-in signal taken for the $\text{VO}_2/\text{Al}_2\text{O}_3(\text{C})$ film. Pump beam crossing angle $\theta=9^\circ$.

signal variation becomes slower. Here, the transition time τ_u is defined for the UPT and indicated by arrows in Fig. 10.

The UPT time was measured as $\tau_u=140 \text{ fs}$, 200 fs , and 450 fs for $\text{VO}_2/\text{Al}_2\text{O}_3(\text{R})$, $\text{VO}_2/\text{Al}_2\text{O}_3(\text{C})$, and VO_2/SiO_2 samples, respectively. These values were reproducible as long as the pump fluence was kept constant. As discussed above the film structural disorder increases from $\text{VO}_2/\text{Al}_2\text{O}_3(\text{R})$ to $\text{VO}_2/\text{Al}_2\text{O}_3(\text{C})$ to VO_2/SiO_2 films; τ_u was found to increase in a parallel way.

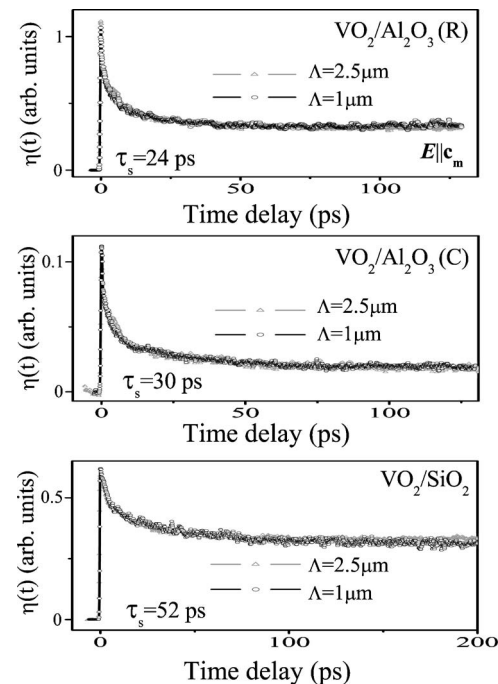


FIG. 11. Transient grating signal versus probe-pulse delay at pump beam crossing angles $\theta=9^\circ$ and $\theta=22.5^\circ$ and grating periods $\Lambda=2.5 \mu\text{m}$ and $\Lambda=1 \mu\text{m}$, respectively, for VO_2 films on different substrates.

After the UPT the diffracted signal undergoes slow decay for tens of picoseconds (Fig. 11) due to the gradual decrease of the grating contrast caused by the I - M PT in the dark areas of the fringe pattern. The recovery process back to the insulator phase occurs after a ~ 250 -ps delay⁴³ and takes several hundreds of nanoseconds. The latter process is beyond the experimental range and to be excluded from the discussion. The relaxation behavior in Fig. 11 is nearly exponential and is common for ultrathin VO₂ films with thicknesses less than ~ 50 nm. The characteristic PT time τ_s is defined as the time when the diffraction signal decays by a factor of $1/e^2$.⁴⁴ The time τ_s was found independent of the grating periods Λ when the crossing angle between the two pump pulses changed. It indicates that on the picosecond time scale, the I - M PT has no significant relation to certain diffusion processes along the grating vector in the film plane.

The general peculiarities of phonon dynamics during a light-induced PT was discussed in Ref. 8. Cavalleri *et al.* pointed out that photoexcited electrons can modify the vibrational spectrum of VO₂ and provide conditions for the PT. In the present work we propose a PT model based on the interaction of excited electronic states with the lattice. Note that there are *three types* of light-induced I - M PT presented below. The first mechanism is related to the UPT dynamics shown in Fig. 10. The second mechanism is also related to the UPT and along with third mechanism to the slower I - M PT characterized by time τ_s (Fig. 11). Each of these processes is elucidated below.

(i) Charge-transfer UPT. As shown in Sec. II, the light-induced UPT occurs at a critical number of photoexcited charge transfers, when condition (8) is satisfied. The final excited state, which is responsible for the mode softening and the I - M UPT, can be attributed to the formation of localized correlated charge-transfer vibronic excitons.³³⁻³⁵ This is bipolaronic charge-transfer excitons, existing under equilibrium between CT's and lattice distortions.

(ii) Wannier-Mott-exciton-controlled PT. It is a cooperative behavior of indirect interactions between vibronic Wannier-Mott excitons (WME's) via phonon modes.^{26,27} Exciton-exciton correlations are here defined as a cooperative "Negative- U " effect which results in a clustering of excitons to form a cooperative excitonic potential well. The well depth increases linearly with concentration n_{WME} of excitons per vibronic WME cluster and can be represented by $\mathcal{E}_{min} = -A - B(T)n_{WME}$. Here A stands for a single vibronic WME energy and the parameter $B(T)$ is related to the cooperative vibronic contribution of all in-cluster excitons to the energy of a single in-cluster WME. The energy of vibronic WME clustering is reduced by this cooperative effect. Consequently, the vibronic WME overlaps with percolation, leading to an increase the effective excitonic radii. The large-radius WME states (V^{5+} +electron in the large-radius state) are rather similar to an intermediate state between insulator and metallic VO₂ with V^{5+} +extended radius electron. At a critical WME density the probability of resonant tunneling into an excited state in the metallic phase becomes greater than exciton decay. This type of PT is caused typically by strong overlapping of these large-radius WME states with the metallic states.

(iii) Phonon-related PT. For the intermediate radii WME's, the phonons generated by laser excitation may

match with the excited vibronic WME states to cause a *resonant interaction*. The multiphonon resonant interaction results in ionization of the vibronic WME's followed by VO₂ lattice transformation. This effect has vibronic origin. In the insulator phase the V^{4+} ionization actually corresponds to $V^{4+} \rightarrow V^{5+} + e_{free}$. Here, the initially occupied $3d_{||}$ state of the V^{4+} ion becomes unoccupied and the deformation field induced by interaction of the $3d_{||}$ state with lattice vibrations disappears. This scenario corresponds to the realization of light-induced ferroelastic PT on picosecond time scale (Fig. 11).

The first two transition mechanisms indicate that the UPT time τ_u strongly depends on excitation power and pulse duration. For disordered VO₂ structure τ_u is expected to increase. For the VO₂/SiO₂ sample (Fig. 10), $\tau_u = 450$ fs was obtained. It is about 3 times longer than that for VO₂/Al₂O₃ due to higher structural disorder in VO₂/SiO₂. Therefore, numerous oxygen vacancies are coexistent with different V charge states. Direct photoexcitation of electrons to oxygen vacancy levels leads to a recharging of the vacancies without the formation of excitonic states. Such a process will reduce the number of photoexcited free carriers and excitons. The presence of structural disorder alters the CT properties, dielectric susceptibility and CT-CT cell-cell interaction energy as well, in consequence of which the UPT time τ_u increases.

The PT time τ_s also increases with VO₂ structural disorder (Fig. 11). Apparently, it is related to the localization of photoexcited carriers in potential wells near defects, resulting in a reduction of the forming cooperative excited states (e.g., cooperative excitonic wells) which are responsible for the PT. Moreover, the slower PT is a transformation of VO₂ domains with monoclinic symmetry to domains with tetragonal symmetry, characterized by displacement of domain walls. The displacement of each domain wall can be significantly reduced due to pinning of the wall by defects.

D. Azimuthal anisotropy of the VO₂ optical response

Transient grating experiments which emphasize the anisotropic properties of VO₂ films were performed with changing sample orientations at fixed delay time τ corresponding to the complete light-induced UPT. The anisotropy of optical properties was only observed in films deposited on single-crystal substrates. The diffraction intensity was found to be dependent on the angle φ between the polarization vector \mathbf{E} of the electromagnetic field and the reference direction. The reference direction for VO₂/Al₂O₃(R) was fixed along the c_m VO₂ axis. For VO₂/Al₂O₃(C), this reference direction cannot be assigned in such a way because of the significant twinning of the VO₂ film on Al₂O₃(C) substrate. Therefore the reference direction was taken as the $[100]_{Al_2O_3(C)}$ direction of the substrate. The measured diffraction signal $\eta(\varphi)$ for different samples was normalized to the maximal signal for VO₂/Al₂O₃(R) and is shown in Fig. 12.

Figure 12(a) shows a significant polarization anisotropy of $\eta(\varphi)$ for VO₂/Al₂O₃(R) while for VO₂/Al₂O₃(C) the angular modulation of $\eta(\varphi)$ is much less noticeable. In general, the signal $\eta(\varphi)$ can be presented as a sum of constant isotropic (η_0) and azimuthal angle-dependent anisotropic [$\Delta\eta(\varphi)$]

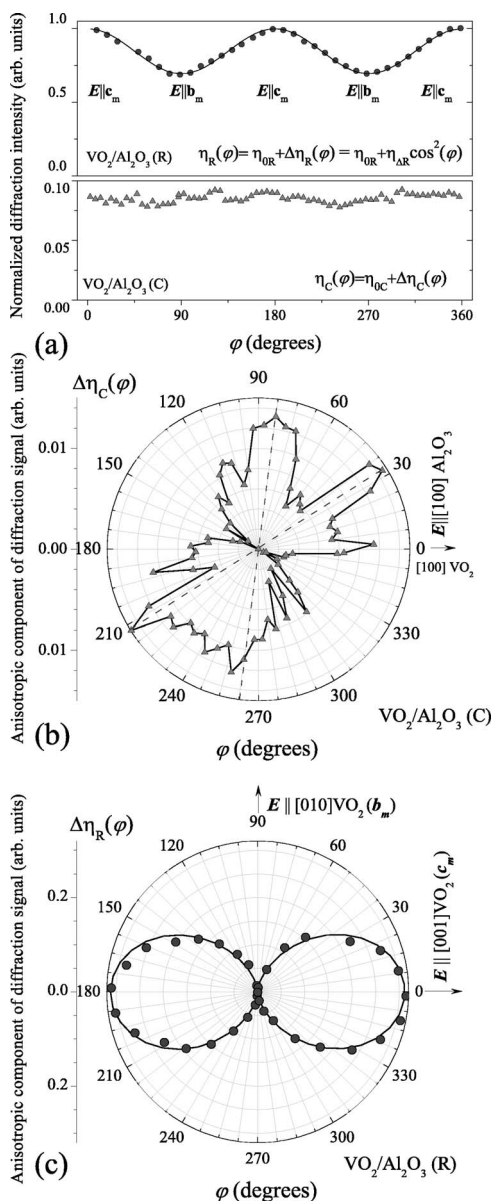


FIG. 12. Diffraction efficiency for $\text{VO}_2/\text{Al}_2\text{O}_3(\text{C})$ and $\text{VO}_2/\text{Al}_2\text{O}_3(\text{R})$ films vs azimuthal direction of light polarization. (a) Total normalized diffraction signal $\eta(\varphi)$; solid line is a fit to $\eta_R(\varphi) = \eta_{0R} + \eta_{\Delta R} \cos^2(\varphi)$. Anisotropic part of diffraction signal: (b) $\Delta\eta_C(\varphi)$ for $\text{VO}_2/\text{Al}_2\text{O}_3(\text{C})$; dotted lines denote orientation of the sample related to the maximal diffraction efficiency. (c) $\Delta\eta_R(\varphi)$ for $\text{VO}_2/\text{Al}_2\text{O}_3(\text{R})$.

components: $\eta(\varphi) = \eta_0 + \Delta\eta(\varphi)$. Anisotropic components $\Delta\eta_C(\varphi)$ for $\text{VO}_2/\text{Al}_2\text{O}_3(\text{C})$ and $\Delta\eta_R(\varphi)$ for $\text{VO}_2/\text{Al}_2\text{O}_3(\text{R})$ are shown in Figs. 12(b) and 12(c), respectively. The modulation of $\Delta\eta_R(\varphi)$ is about 30%, but only $\sim 1\%$ for $\Delta\eta_C(\varphi)$.

As shown above, a general property of $\text{VO}_2/\text{Al}_2\text{O}_3(\text{C})$ is a threefold twinning of the crystalline film with 120° domain walls. The angular distribution of transient grating diffraction signal [Fig. 12(a)] is mostly isotropic due to this film twinning. Nevertheless, the angular distribution of $\Delta\eta_C(\varphi)$ demonstrates a slight anisotropy [Fig. 12(b)] which can be associated with two preferred directions. Since the diffraction signal depends on the film morphology within several tens of

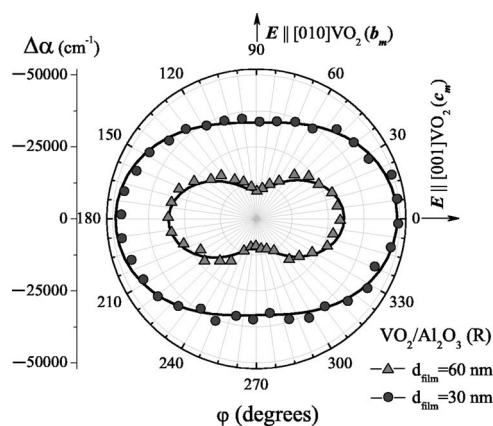


FIG. 13. Azimuthal dependence of the absorption coefficient variations during the *I-M* PT for the 30- and 60-nm-thick VO_2 films deposited on an $\text{Al}_2\text{O}_3(\text{R})$ substrate.

microns illuminated by the probe beam, the $\sim 60^\circ$ anisotropy of $\Delta\eta_C(\varphi)$ indicates that a higher number of $\text{VO}_2/\text{Al}_2\text{O}_3(\text{C})$ domains are oriented along only two directions in the (001) Al_2O_3 plane within the monitored area.

The angular dependence of the normalized diffraction signal for $\text{VO}_2/\text{Al}_2\text{O}_3(\text{R})$ can be fitted by $\eta_R(\varphi) = \eta_{0R} + \eta_{\Delta R} \cos^2(\varphi)$, where $\eta_{0R} = 0.69$ and $\eta_{\Delta R} = 0.31$ are constants. This distribution is elongated along the c_m axis [Fig. 12(c)]. This remarkable optical anisotropy, as well as its narrow temperature hysteresis ($\Delta T \approx 4$ K) and the XRD and AFM data presented before, indicates that the optical and structural properties of the crystalline VO_2 film grown on $\text{Al}_2\text{O}_3(\text{R})$ are closer to those of the bulk single crystal.

During the *I-M* PT the absorption coefficient of bulk VO_2 increases. Nevertheless, in thin VO_2 films the absorption by the film decreases due to an interference effect. The change of the effective absorption coefficient can be expressed as $\Delta\alpha = -(1/d_{\text{film}}) \ln(I'/I^m)$, where I' and I^m are the transmitted intensities for the film in tetragonal and monoclinic phases, respectively. The light-induced change in transmission for $\text{VO}_2/\text{Al}_2\text{O}_3(\text{R})$ films with 30 and 60 nm thicknesses was measured at a fixed delay time τ with various sample orientations. Data obtained for the absorption coefficient variations demonstrate significant angular anisotropy (Fig. 13).

The indices of refraction for the two orthogonal crystallographic directions of the $\text{VO}_2/\text{Al}_2\text{O}_3(\text{R})$ film were calculated from the data shown in Fig. 13. Additional measurements of the reflection coefficient have been also conducted in order to reduce the numerical error. A thin film model⁴⁰ was used in the calculation procedure. In the monoclinic phase the index of refraction for $[010]\text{VO}_2$ (b_m) and $[001]\text{VO}_2$ (c_m) directions was found to be $n_o = 2.87 + i1.13$ and $n_e = 2.95 + i1.16$, respectively, at $\lambda = 400$ nm. After the light-induced PT, due to the relative isotropy of optical constants in the higher-symmetry tetragonal phase, only a weak polarization dependence of transmission and reflection was found. The averaged index of refraction obtained for the metallic tetragonal phase is $n_m = 2.5 + i1.17$.

The optical absorption of vanadium dioxide could significantly change the optical indicatrix. On the other hand, in thin VO_2 film the real part of the refractive index provides a

significant contribution to the film absorption. Moreover, the imaginary part of the VO₂ refractive index is about 2 times less than the real part and the relative change of the imaginary part is significantly smaller at $\lambda=400$ nm. This result indicates that the dominant contribution to the VO₂ optical response during the PT is due to variation in the real part of the refractive index.

As shown in Fig. 12(a), due to significant twinning of VO₂/Al₂O₃(C), the optical properties of this film are mostly isotropic. On the other hand, the VO₂/Al₂O₃(R) properties are similar to those of single VO₂ crystal. The XRD data show that the (100)VO₂ plane is parallel to the substrate and two crystallographic directions b_m and c_m are in the surface plane. The angle between the y and c_m axes is $\varphi_m=32.61^\circ$ (Fig. 1). As a result, at normal incidence of the laser pulse the angle between the optical axis z and wave vector \mathbf{k} is φ_m . In the VO₂ crystal $\mathbf{k}=(2\pi n/\lambda)\mathbf{s}$, where n is the index of refraction, and \mathbf{s} is the unit vector. The refractive indices which correspond to ordinary and extraordinary waves in the crystal can be found by solving the equation⁴⁵

$$\det|n^2(\delta_{ij} - s_i s_j) - \varepsilon_{ij}| = 0. \quad (12)$$

Here $i, j=x, y, z$; δ_{ij} is the unit tensor. The cross section of the optical indicatrix by surface plane parallel to (100)VO₂ is an ellipse with two axes along b_m and c_m . Only the ordinary wave propagates through the crystal when light polarization is along the b_m axis ($\mathbf{E}\parallel b_m$). When $\mathbf{E}\parallel c_m$, only the extraordinary wave propagates through the crystal in the (010) plane. Dielectric constants for VO₂/Al₂O₃(R) can be found by solving Eq. (12). Taking into account the relation $\varepsilon=n^2$ and that $\varphi_m\approx 30^\circ$, the dielectric constants ε_o^t and ε_e^t in the tetragonal phase for two corresponding orthogonal directions b_m and c_m are

$$\varepsilon_o^t = \varepsilon_\perp^t, \quad \varepsilon_e^t = \frac{\varepsilon_\perp^t \varepsilon_\parallel^t}{\varepsilon_\perp^t \sin^2 \varphi_m + \varepsilon_\parallel^t \cos^2 \varphi_m} \approx \frac{4\varepsilon_\perp^t \varepsilon_\parallel^t}{\varepsilon_\perp^t + 3\varepsilon_\parallel^t}. \quad (13)$$

Analogous values ε_o^m and ε_e^m for the monoclinic phase are

$$\varepsilon_o^m = \varepsilon_{xx}^m, \quad \varepsilon_e^m = \frac{\varepsilon_{yy}^m \varepsilon_{zz}^m - \varepsilon_{yz}^m{}^2}{\varepsilon_{yy}^m \sin^2 \varphi_m + \varepsilon_{zz}^m \cos^2 \varphi_m + \varepsilon_{yz}^m \sin 2\varphi_m} \\ \approx \frac{4(\varepsilon_{yy}^m \varepsilon_{zz}^m - \varepsilon_{yz}^m{}^2)}{\varepsilon_{yy}^m + 3\varepsilon_{zz}^m + 2\sqrt{3}\varepsilon_{yz}^m}. \quad (14)$$

Thus, in according to Eq. (11) the angular dependence of the transient grating diffraction signal for VO₂/Al₂O₃(R) can be expressed as

$$\eta(\varphi) \approx \text{OF} \langle |\Delta\varepsilon_o(t)|^2 \rangle \\ \times \left[1 + \cos^2 \varphi \left(\frac{\langle |\Delta\varepsilon_e(t)|^2 \rangle - \langle |\Delta\varepsilon_o(t)|^2 \rangle}{\langle |\Delta\varepsilon_o(t)|^2 \rangle} \right) \right], \quad (15)$$

where φ is the angle between the polarization vector \mathbf{E} and c_m axis, and $\Delta\varepsilon_o=(\varepsilon_o^t-\varepsilon_o^m)$ and $\Delta\varepsilon_e=(\varepsilon_e^t-\varepsilon_e^m)$. Since the normalized signal [Figs. 12(a) and 12(c)] has azimuthal depen-

dence $\eta_R(\varphi)=\eta_{0R}+\eta_{\Delta R}\cos^2(\varphi)$, the ratio $|\Delta\varepsilon_o|/|\Delta\varepsilon_e|$ can be estimated as

$$\frac{|\Delta\varepsilon_o|}{|\Delta\varepsilon_e|} \approx \sqrt{\frac{\langle |\Delta\varepsilon_o|^2 \rangle}{\langle |\Delta\varepsilon_e|^2 \rangle}} = \sqrt{\eta_{0R}} = \sqrt{1 - \eta_{\Delta R}}. \quad (16)$$

Analysis of experimental diffraction data gives the value $|\Delta\varepsilon_o|/|\Delta\varepsilon_e|=0.83$. A similar value $|\Delta\varepsilon_o|/|\Delta\varepsilon_e|=0.82$ was calculated from the optical constants obtained in transmission pump-probe measurements discussed above. Thus, these two results obtained in different optical experiments are consistent. Therefore, the transient grating signal for thin VO₂/Al₂O₃(R) film can be correctly described by (11) and (15) and it gives reliable information about the relative change of the dielectric constants.

The transient grating diffraction signal [Figs. 10–12] as well as the transmission change during a thermally induced PT (Fig. 9) for VO₂/Al₂O₃(C) is much smaller than for VO₂/Al₂O₃(R). By comparison of data obtained for these samples, one can suppose that the change of ε_{xx} and ε_{yy} components of the VO₂ dielectric tensor upon a PT is much larger than ε_{zz} or ε_{yz} at $\lambda=400$ nm. Taking into account (13)–(15), it is very likely that the pronounced optical response of VO₂/Al₂O₃(R) occurs mainly due to a significant change in the ε_{xx} and ε_{yy} components. In terms of the charge-transfer model, the major contribution to the electronic susceptibility is produced by the V-O-V CT process. It should be noticed that the angular distribution of transmission, reflection, and transient grating diffraction signal for metallic VO₂/Al₂O₃(R) at sample temperature $T=410$ K was almost isotropic. Hence, the angular anisotropy in optical signal for VO₂/Al₂O₃(R) is apparently due to different conditions for V-O-V CT along the a_t and b_t axes in the monoclinic phase (Figs. 1 and 2). While in the tetragonal phase the parameters for CT along the a_t and b_t axes are equivalent, in the monoclinic phase it is certainly not due to differing interatomic distances along corresponding axes.

V. CONCLUDING REMARKS

Using the transient grating technique and spectral transmission and reflection, the light-induced insulator-to-metal phase transition in VO₂ crystalline films was characterized. The observed PT in different VO₂ films suggests that the phase transition time and excited-state relaxation dynamics depend on the film structure, concentration of oxygen vacancies, and other structural defects. Most likely, the increase of oxygen vacancy concentration and lattice disorder decrease the PT rate. The light-induced PT is attributed to the charge-transfer and exciton-controlled mechanism.

The charge-transfer model is proposed to describe the VO₂ dielectric susceptibility. The present analysis can be extended to other solid-state materials.

Comparison of spectral reflectivity variations upon a light-induced and thermally induced PT clearly shows that photoexcitation of VO₂ results in complete insulator-to-metal PT. After the PT produced by the laser pulse, the nonlinear contribution of nonequilibrium carriers to the transient optical properties of VO₂ is insignificant. A transient optical re-

sponse occurs mainly due to the change in linear susceptibility.

VO₂ films prepared for this optical study exhibit significantly different morphology, depending on their substrates. While VO₂ on amorphous SiO₂ substrate is statistically isotropic, with numerous structural defects, the crystalline VO₂ films on single-crystal sapphire substrates have preferable orientation along sapphire crystallographic directions and a relatively low concentration of defects. The x-ray diffraction analysis, atomic force microscopy, and optical experiments show nontwinned structure for VO₂/Al₂O₃(R), with optical properties closer to bulk single-crystal VO₂. The VO₂ film deposited on an Al₂O₃(C) substrate is significantly twinned, with crystallites oriented along three crystallographic directions of the substrate and 120° domain walls. Nevertheless, local orientation of VO₂ grains was found only along two directions for small regions sampled in the optical experiments.

An important result of this experimental study shows the significant polarization dependence of the transient grating

diffraction intensity and pump-probe transient transmission for the VO₂/Al₂O₃(R) film. It showed that the light-induced change of dielectric constants during a PT is anisotropic which can be observed by the pump-probe technique and analyzed by an optical indicatrix for single-crystal VO₂. The VO₂ crystalline film deposited on an Al₂O₃(C) substrate demonstrates only slight anisotropy in the transient grating diffraction signal due to significant twinning of the film. Finally, the substantial anisotropic ultrafast response of crystalline VO₂ films will find a wide variety of applications in ultrafast polarization holography, diffractive optics, intracavity mirrors of pulsed lasers, and information processing.

ACKNOWLEDGMENTS

The authors acknowledge funding from US-DOD-W911NF-04-1-0019, NSF-EPSCoR, and ARO-DAAD19-02-1-0298.

*Permanent address: A.F. Ioffe Physical Technical Institute, St. Petersburg 194021, Russia.

†Corresponding author. Electronic address: hliu@uprm.edu

¹F. J. Morin, Phys. Rev. Lett. **3**, 34 (1959).

²A. Cavalleri, Cs. Tóth, C. W. Siders, J. A. Squier, F. Raksi, P. Forget, and J. C. Kieffer, Phys. Rev. Lett. **87**, 237401 (2001).

³H. W. Verleur, A. S. Barker, Jr., and C. N. Berglund, Phys. Rev. **172**, 788 (1968).

⁴C. N. Berglund and H. J. Guggenheim, Phys. Rev. **185**, 1022 (1969).

⁵A. S. Barker, Jr., H. W. Verleur, and H. J. Guggenheim, Phys. Rev. Lett. **17**, 1286 (1966).

⁶J. P. Pouget, H. Launois, T. M. Rice, P. Dernier, A. Gossard, G. Villeneuve, and P. Hagemuller, Phys. Rev. B **10**, 1801 (1974).

⁷J. C. Rakotoniaina, R. Mokrani-Tamellin, J. R. Gavari, G. Vacquier, A. Casalot, and G. Galvarin, J. Solid State Chem. **103**, 81 (1993).

⁸A. Cavalleri, Th. Dekorsy, H. H. W. Chong, J. C. Kieffer, and R. W. Schoenlein, Phys. Rev. B **70**, 161102(R) (2004).

⁹S. Chen, H. Ma, X. Yi, H. Wang, X. Tao, M. Chen, X. Li, and C. Ke, Infrared Phys. Technol. **45**, 239 (2004).

¹⁰I. Balberb and S. Trokman, J. Appl. Phys. **46**, 2111 (1975).

¹¹J. C. C. Fan, H. R. Fetterman, F. J. Bachner, P. M. Zavrasky, and C. D. Parker, Appl. Phys. Lett. **30**, 11 (1977).

¹²S. A. Pollack, D. B. Chang, F. A. Chudnovsky, and I. A. Khakhaev, J. Appl. Phys. **78**, 3592 (1995).

¹³V. L. Gal'perin, I. A. Khakhaev, F. A. Chudnovski, and E. B. Shadrin, Zh. Tekh. Fiz. **43**, 235 (1998).

¹⁴O. B. Danilov and A. I. Sidorov, Tech. Phys. **44**, 1345 (1999).

¹⁵N. F. Bochorishvili, V. D. Vvedenskii, Yu. M. Gerbshtein, O. B. Danilov, V. A. Klimov, N. Yu. Sentsov, F. A. Chudnovskii, and E. B. Shadrin, Sov. Phys. Tech. Phys. **34**, 1140 (1989).

¹⁶D. Paquet and P. Leroux-Hugon, Phys. Rev. B **22**, 5284 (1980).

¹⁷S. Biermann, A. Poteryaev, A. I. Lichtenstein, and A. Georges, Phys. Rev. Lett. **94**, 026404 (2005).

¹⁸H. Liu, R. C. Powell, and L. A. Boatner, Phys. Rev. B **44**, 2461 (1991).

¹⁹H. Liu, R. J. Reeves, R. C. Powell, and L. A. Boatner, Phys. Rev. B **49**, 6323 (1994).

²⁰M. Gupta, A. J. Freeman, and D. E. Ellis, Phys. Rev. B **16**, 3338 (1977).

²¹H. Terauchi and J. B. Cohen, Phys. Rev. B **17**, 2494 (1978).

²²J. B. Goodenough, J. Solid State Chem. **3**, 490 (1971).

²³V. Eyert, Ann. Phys. **11**, 650 (2002).

²⁴E. Caruthers and L. Kleinman, Phys. Rev. B **7**, 3760 (1973).

²⁵V. S. Vikhnin, S. Lysenko, A. Rua, F. Fernandez, and H. Liu, Phys. Lett. A **343**, 446 (2005).

²⁶V. S. Vikhnin, S. Lysenko, A. Rua, F. Fernandez, and H. Liu, J. Phys.: Condens. Matter **21**, 44 (2005).

²⁷V. S. Vikhnin, S. Lysenko, A. Rua, F. Fernandez, and H. Liu, Solid State Commun. **137**, 615 (2006).

²⁸S. Westman, Acta Chim. Acad. Sci. Hung. **15**, 217 (1961).

²⁹A. D. Burton and P. A. Cox, Philos. Mag. B **51**, 2 (1985).

³⁰G. Anderson, Acta Chem. Scand. (1947-1973) **10**, 623 (1956).

³¹M. Born and E. Wolf, *Principles of Optics: Electromagnetic Theory of Propagation, Interference, and Diffraction of Light* (Cambridge University Press, Cambridge, England, 1999).

³²R. Heckingbottom and J. V. Lennett, Nature (London) **194**, 678 (1962).

³³V. Vikhnin, Ferroelectr., Lett. Sect. **25**, 27 (1999).

³⁴V. S. Vikhnin, R. I. Eglitis, S. E. Kapphan, E. A. Kotomin, and G. Borstel, Europhys. Lett. **56**, 702 (2001).

³⁵V. S. Vikhnin, R. I. Eglitis, S. E. Kapphan, G. Borstel, and E. A. Kotomin, Phys. Rev. B **65**, 104304 (2002).

³⁶Z. P. Wu, S. Yamamoto, A. Miyashita, Z. J. Zhang, K. Narumi, and H. Naramoto, J. Phys.: Condens. Matter **10**, L765 (1998).

³⁷M. Borek, F. Qian, V. Nagabushnam, and R. K. Singh, Appl. Phys. Lett. **63**, 3288 (1993).

³⁸J. M. Bennett and L. Mattsson, *Introduction to Surface Roughness and Scattering* (Optical Society of America, Washington, D.C.,

- 1989).
- ³⁹V. A. Klimov, I. O. Timofeeva, S. D. Khanin, E. B. Shardin, A. V. Ilinskii, and F. Silva-Andrade, *Tech. Phys.* **47**, 1134 (2002).
- ⁴⁰R. M. A. Azzam and N. M. Bashara, *Ellipsometry and Polarized Light* (North-Holland, Amsterdam, 1977).
- ⁴¹I. M. Fishman, C. D. Marshall, J. S. Meth, and M. D. Fayer, *J. Opt. Soc. Am. B* **8**, 1880 (1991).
- ⁴²J. M. Elson, *Waves Random Media* **7**, 303 (1997).
- ⁴³S. Lysenko, V. S. Vikhnin, G. Zhang, A. Rua, F. Fernandez, and H. Liu, *Proc. SPIE* **6170**, 61701R (2006).
- ⁴⁴A. M. Ghazzawi, J. K. Tyminski, R. C. Powell, and J. C. Walling, *Phys. Rev. B* **30**, 7182 (1984).
- ⁴⁵L. D. Landau and E. M. Lifshitz, *Electrodynamics of Continuous Media* (Pergamon, Oxford, 1975).